THE INTERACTION WITH LIGHT OF PHONONS IN SELENIUM

R. Zallen and G. Lucovsky

pp. 148-173 in *Selenium*, edited by R.A. Zingaro and W.C. Cooper (Van Nostrand/Reinhold, New York, 1974).

4

The Interaction with Light of Phonons in Selenium*

RICHARD ZALLEN/GERALD LUCOVSKY
Xerox Research Laboratories, Rochester, N.Y.

INTRODUCTION

This article reviews those optical properties of selenium which are determined by the atomic vibrations of the crystal or glass lattice. While we have collected for discussion some of the most important experimental and theoretical results, our emphasis will be on the qualitative features and the physical significance of the data, rather than on the numerical values of the parameters presented.

We will discuss the three principal allotropic forms of solid selenium: two crystalline modifications, trigonal Se and α-monoclinic Se; and the important amorphous modification as well. The pertinent experiments are, primarily, measurements of infrared absorption and of Raman scattering. Because we are concerned with those lattice waves (phonons) which interact with incident light waves (photons), which possess small wave-

* See also Chapter 5.

vectors ($\mathbf{q} \sim \omega/c$), the phonons involved are those near the center of the Brillouin zone ($\mathbf{q} \approx 0$, the vibrational "long waves").[2]

For any solid, a knowledge of the vibrations of the atoms about their equilibrium lattice positions is of great interest because of the insight gained into the interatomic bonding interactions, which are responsible for the very existence of the solid and for the particular structure it assumes. For selenium, however, the lattice optical properties are of special added significance due to the occurrence of reststrahlen, one-phonon absorption bands in the far-infrared which are produced by the strong, direct interaction of light with lattice fundamentals. This interaction, which is customarily associated with ionic crystals and is widely (and mistakenly) assumed to be absent in elemental solids, occurs in all three forms of Se. Trigonal Se, the most extensively studied of the three, is very special since it is, as we shall see, *the simplest reststrahlen-displaying elemental crystal.*

Because of its unique position with respect to the photon-phonon interaction and the fact that the available experimental information is most complete for this material, trigonal Se is reviewed in some detail. As a prerequisite for the interpretation of the experiments, the symmetry and the consequent optical selection rules are presented in the next section. The coupled photon-phonon spectra of trigonal Se are discussed later with particular emphasis on the responsible underlying mechanism of dynamic charge. Higher order phonon-involving optical interactions in this crystal, particularly Raman scattering and two-phonon infrared absorption, are then reviewed.

The covalent coordination of selenium is twofold, and as a consequence of this low coordination, it forms molecular crystals rather than network crystals. In trigonal Se, the molecular unit is an extended chain; in monoclinic Se, an eight-membered ring. The recent work on the two crystal forms has permitted an analysis of the spectra of the vitreous form in terms of vibrations of these two types of molecular structural units. The spectra of the glass are found to be dominated by features ascribable to Se_8 molecules, providing direct evidence for the presence of this molecular species in significant concentrations in amorphous Se. The lattice spectra of monoclinic Se are discussed elsewhere as well as the spectra and structure of amorphous Se.

SYMMETRY AND SELECTION RULES FOR TRIGONAL Se

The three-atom unit cell of trigonal Se and Te is shown in Figure 4-1. The crystal structure[36] consists of helical coils ("chains") which wind around axes parallel to the crystalline c-axis, which is a triad screw axis. The helices contain three atoms per turn and are in hexagonal array (close packing for rods). The space group is $P3_121$ (D_3^4) for the right-handed crystal of Figure

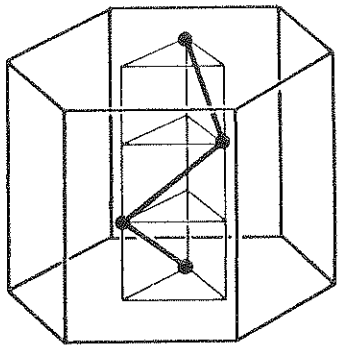

Figure 4-1 Unit cell for the crystal structure of trigonal Se, slightly schematized to clearly reveal the chain structure.

4-1. For the enantiomorphic left-handed form, the space group is $P3_221$, or D_3^6. This is the same symmetry which applies to quartz and to cinnabar (trigonal HgS[39]); Se and Te are monatomic analogues of those crystals. This is the least complex crystal structure based on a helix. For example, these are the simplest crystals (elemental crystals, triatomic unit cell) which exhibit circular dichroism and optical activity.

Se and Te are molecular crystals with the molecular unit, the helical chain, infinitely extended in one dimension. Viewed in this way, they are clearly prototype polymers. The intermolecular bonding between chains is much weaker than the molecular bonding within each chain; the ratio between the smallest chain-chain and intrachain bond lengths is 1.49 for Se and 1.31 for Te. The weak interchain bonding is markedly manifest in the cleavage behavior; the crystals cleave only in planes containing the c-axis (no broken chains). To our knowledge, these are the only elemental crystals with three atoms in the primitive unit cell. As will be discussed further on, this makes them unique with respect to the interaction with light of their lattice vibrations.

The six operations of the factor group for D_3^4 crystals are 1, 3_1, $3_1 \times 3_1$, 2, $3_1 \times 2$, and $2 \times 3_1$, where:

1 denotes the identity
3_1 denotes a threefold rotation about the c-axis, followed by a $(1/3)c$ translation parallel to the axis
2 denotes a twofold rotation about an axis perpendicular to c

This group has been discussed by several researchers.[1,17,25] It is simply isomorphic to the familiar point group $3m$ (C_{3v}) of the equilateral triangle and possesses three irreducible representations (I.R.'s): A_1, A_2, and E. A_1 and A_2 are one-dimensional symmetric and antisymmetric representations with respect to the twofold rotations, and E is a two-dimensional representation.

Notations other than A_1, A_2, and E which have also been used for the Γ-point ($\mathbf{q} = 0$) I.R.'s are Γ_1, Γ_1', Γ_2[17] and Γ_1, Γ_2, Γ_3.[1] The character table for the group is contained in Table 4-1.

The symmetries of the long wavelength phonons are determined by Γ, the factor-group representation generated by the displacements of the atoms in the unit cell. For trigonal Se, Γ is 9-dimensional and is, of course, reducible. The characters for Γ are shown in the fourth row of Table 4-1, and its reduction into I.R.'s is given in the fourth column: $\Gamma = A_1 + 2A_2 + 3E$. Also listed is the three-dimensional polar-vector representation P. The three zone-center acoustical phonons (rigid translations of the crystal) comprise such a representation, so that the I.R.'s of the optical phonons are contained in $\Gamma - P = A_1 + A_2 + 2E$. Thus, there are four optical-mode eigenfrequencies (ignoring for the moment the transverse-longitudinal splitting of the infrared-active vibrations) corresponding to two nondegenerate A modes ($A_1 + A_2$), and two doubly-degenerate pairs of E modes. The eigenvectors for the nondegenerate optical vibrations are determined by symmetry. The A_1 mode is a breathing mode of the helical chains, the A_2 mode is a chain-rotational mode (to be discussed in another section).

Symmetry-determined selection rules governing the interaction of these vibrations with light are presented in the last two columns of Table 4-1. For one-phonon optical absorption, the mode must induce a first-order electric moment $\mathbf{p}$, so that it necessarily transforms as a vector. The infrared-active modes are therefore those of symmetry types common to $\Gamma - P$ and P; the I.R.'s contained in this intersection are A_2 and E. The A_2-symmetry optical

TABLE 4-1 SYMMETRY ANALYSIS AND SELECTION RULES FOR THE ZONE-CENTER PHONONS IN TRIGONAL Se

Representation		Class Characters 1	3_z	2_x	Zone-Center Modes All Acoust. Opt. Γ	P	$\Gamma - P$	Selection Rules Infrared	Raman
Irred reps (I.R.)	A_1	1	1	1	1	0	1	—	$\alpha_{zz}, \alpha_{xx} + \alpha_{yy}$
	A_2	1	1	−1	2	1	1	p_z	—
	E	2	−1	0	3	1	2	p_x, p_y	$\alpha_{xy}, \alpha_{yz}, \alpha_{zx}, \alpha_{xx} - \alpha_{yy}$
Unit-cell rep.	Γ	9	0	−1					
Vector rep	P	3	0	−1					

Two-phonon combinations

$A_1 \times A_1 = A_2 \times A_2 = A_1$,	Raman
$A_1 \times A_2 = A_2$,	IR (z);
$A_1 \times E = A_2 \times E = E$,	IR (x, y) and Raman;
$E \times E = A_1 + A_2 + E$,	IR (x, y, z) and Raman.

mode interacts with light polarized parallel to the c-axis (c-axis = the z axis of Table 4-1); the E modes interact with light polarized perpendicular to c. The nature of these interactions is explored in the following section.

The symmetric A_1 vibration, which does not interact with light in first-order and is therefore absent from the fundamental infrared spectrum, can be acquired in Raman scattering. A Raman-active vibration induces a first-order modulation in the dielectric polarizability tensor at optical frequencies, so that it must transform as a component of a symmetric second-rank tensor. The Raman selection rules for D_3 symmetry are given in the last column of Table 4-1. The E modes, as well as the A_1, are permitted in Raman scattering. The presence of vibrations entitled to appear in both the Raman and infrared spectra, the E modes, is permitted by the absence of inversion symmetry. For completeness, the lower part of Table 4-1 shows two-phonon selection rules for combination bands produced by pairs of zone-center phonons. Both Raman scattering spectra and two-phonon absorption spectra for trigonal Se will be discussed.

THE PHOTON–PHONON INTERACTION IN TRIGONAL Se

Reststrahlen in Elemental Crystals

The phenomenon of reststrahlen, the intense absorption of light by a crystal in the far infrared which is produced by strong interaction with lattice vibration fundamentals (single phonons), is one of the most familiar effects in the spectroscopy of solids. Reststrahlen bands are normally associated with ionic crystals, NaCl being the classic prototype.[2] In fact, the oscillating electric dipole moment set up by the lattice vibrations, which gives rise to the strong photon-phonon interaction, is often interpreted as an entirely ionic effect. This, however, is not true. If it were, then crystals composed of a single atomic species, elemental crystals such as Se, could not exhibit reststrahlen because of the absence of ionic charge. The widespread incorrect idea[3,23] that an elemental crystal cannot exhibit one-phonon optical absorption has been reenforced by the circumstance that for the familiar Group IV diamond-structure semiconductors (C, Si, Ge, α-Sn), the zone-center optical phonons are indeed infrared-inactive; they do not couple to light. The explanation of this inactivity is, however, based on a symmetry consideration and is *not* because these are homopolar covalent solids. In general, lattice vibrations in elemental crystals *can* possess a first order electric moment, and thus exhibit reststrahlen, by the mechanism of displacement-induced charge redistribution (*dynamic charge*[7,10,11]).

All crystalline compounds possess infrared-active lattice fundamentals, but not all elemental crystals do. The reason for the nonoccurrence of reststrahlen

in diamond-structure crystals, as first stated by Lax and Burstein[18] in 1955, is discussed in a recent article by Zallen[37] in which the following generalization is derived:

> *A necessary and sufficient condition for the existence of reststrahlen in an elemental crystal is a structure with at least three atoms in the primitive unit cell,* $s \geqslant 3$.

For Ge and Si $s = 2$, so that the optical modes are infrared-inactive. The crystal structure of trigonal Se and Te (Figure 4-1), with $s = 3$, is the simplest structure known to occur which satisfies this minimum complexity condition for a reststrahlen-displaying elemental crystal. In other words, among elemental crystals, Ge and Si are structurally too simple to display the phenomenon under consideration; Se and Te have just the minimum amount of structural complexity ($s = 3$) necessary to exhibit it.

Trigonal Se displays pronounced reststrahlen bands. These form the subject of the following two sections. The underlying mechanism for the lattice-wave–electromagnetic-wave interaction and the experimentally-observed spectra are also reviewed. The photon-phonon interaction in Se is of particular special significance because, as mentioned previously, this material shares with Te the distinction of being structurally *the simplest known reststrahlen-displaying elemental crystal.*

Dynamic Charge in Trigonal Se

For one-phonon optical absorption, a zone-center ($\mathbf{q} \approx 0$) vibration must exhibit a first-order moment, a macroscopic polarization $\boldsymbol{p}$ linear in the atomic displacements $\mathbf{u}$. The mechanism for the first-order moment in an elemental crystal is schematically illustrated in a one-dimensional model in Figure 4-2d; we introduce it with a prerequisite discussion of a one-dimensional representation of NaCl in Figure 4-2a and Figure 4-2b.

Figure 4-2a shows NaCl in the rigid ion model. In this model the effective charge e^* connecting $\mathbf{u}$ and $\boldsymbol{p}$ is just e, the static ionic charge residing on and moving with each ion. However, it is well known that for the alkali halides, e^*/e is appreciably smaller than 1 because of the deformability of the halogen ions. The effects of dynamic charge, the deformability of ions under atomic displacements, is illustrated in Figure 4-2b–Figure 4-2d by means of the shell model, in which the ions are resolved into rigid oppositely-charged cores and shells. The shell model was originally introduced by Dick and Overhauser[12] in order to elucidate, in a simple manner, the role of dynamic charge in the alkali halides in producing the deviation of e^*/e from 1, the rigid-ion value for these crystals. How this comes about is indicated in Figure 4-2b. Recently, Chen and Zallen[10,38] applied the shell model to Se

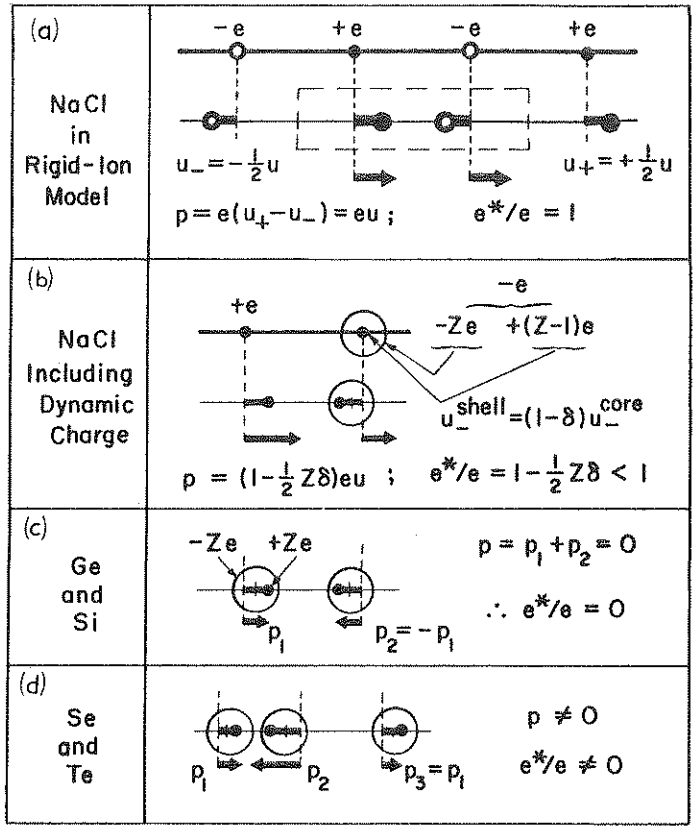

Figure 4-2 One-dimensional representations of the mechanisms for the vibration-induced first-order electric moment responsible for reststrahlen: (a) rigid-ion model for a diatomic ionic crystal; (b) effect of dynamic charge for NaCl; (c) dynamic charge in Ge and Si; and (d) dynamic charge in Se and Te.

and Te in order to elucidate the manner in which charge deformation produces the observed deviation of e^*/e from *zero*, the rigid-ion value for elemental crystals. The dynamic charge in ionic crystals plays the role of a correction; in elemental crystals it is the whole story.

The basic feature of the dynamic-charge mechanism for Se is shown in Figure 4-2d. For Se and Te, and for Ge and Si (shown in Figure 4-2c) as well, dynamic charge produces an induced electric dipole at each atomic site. For Ge and Si, as for all elemental crystals with $s = 2$, the two induced dipoles within the unit cell are required by symmetry to be equal and opposite.[18,37] There is no net unit-cell electric moment, hence no reststrahlen. For Se and Te there is no corresponding constraint. The net moment does not vanish

and these crystals exhibit strong reststrahlen bands, with values of e^*/e on the order of unity. We shall consider here in more detail the dynamic charge associated with the simplest of the infrared-active vibrations of trigonal Se.

From Table 4-1 we see that the A_2-symmetry zone-center optical phonon in Se is responsible for the reststrahlen band observed with light polarized parallel to the trigonal c-axis. The eigenvector for this nondegenerate vibration is determined by symmetry alone; it is a chain-rotational vibration in which intrachain bond lengths and angles are preserved. The first-order electric moment for this mode is illustrated in Figure 4-3, following the shell-model treatment of Chen and Zallen. The macroscopic polarization resides

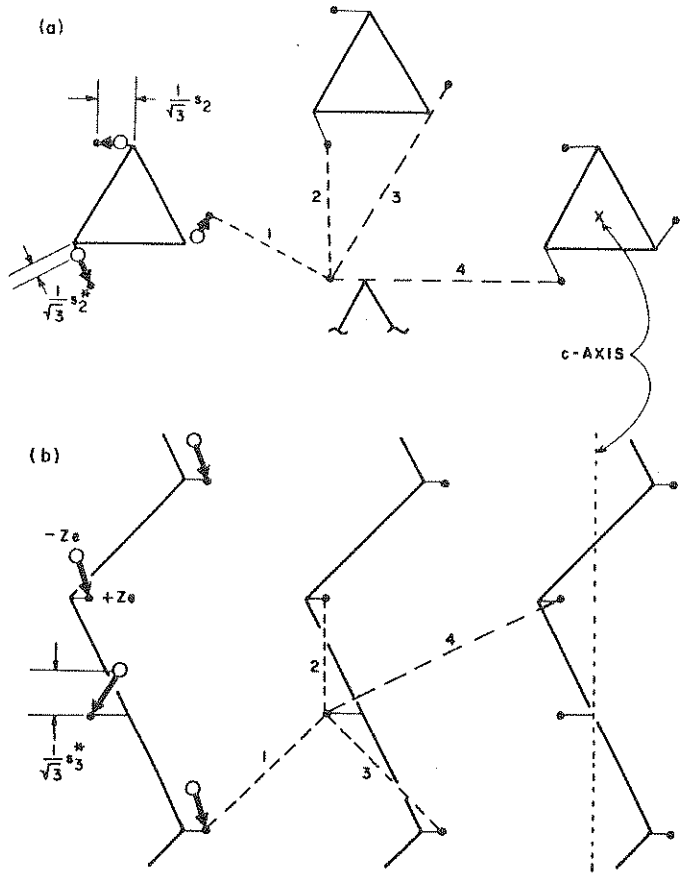

Figure 4-3 Shell-model picture for the dynamic charge electric moment, p_z, of the A_2-symmetry optical mode in trigonal Se: (a) top view, viewed along the c-axis; (b) side view, viewed $\perp$ c. Solid dots represent displaced cores; open circles represent displaced shells.[10]

with the axial shell displacements (indicated by s_3^* in the figure) induced by the chain-twisting atomic displacements (indicated by s_2). Figure 4-3 accounts for the remarkable circumstance that a vibration with all of the atomic displacements perpendicular to c interacts with radiation polarized parallel to c. For this mode both the dynamic charge and the restoring force depend upon the presence of intermolecular interactions between chains, and vanish in the limit of isolated chains.

The Reststrahlen and Polariton Spectra

The far-infrared reflectivity spectra of trigonal Se have been measured by Lucovsky *et al.*[21] and by Geick *et al.*,[15] with essentially similar results. The reststrahlen spectra for the two independent polarizations are shown in Figure 4-4. The high-frequency E mode, infrared-active for $E \perp c$, is off scale to the right of the range shown; it is much weaker than the other bands and is definitively determined in transmission measurements. The infrared spectra were fitted with a set of classical oscillators, each contributing a term of the form $s\bar{\nu}_t^2/(\bar{\nu}_t^2 - \bar{\nu}^2 + i\gamma\bar{\nu}_t\bar{\nu})$ to the complex dielectric constant $\varepsilon(\bar{\nu})$. For a given oscillator, $\bar{\nu}_t$ is the oscillator frequency (transverse frequency in wavenumber units), s is the oscillator strength (contribution of the absorption band to the static dielectric constant), and γ is the dimensionless damping parameter. The oscillator parameters for the A_2 and E modes are listed in Table 4-2. Also included in this table, for completeness, is the A_1 eigenfrequency obtained from the Raman-scattering experiments to be discussed in

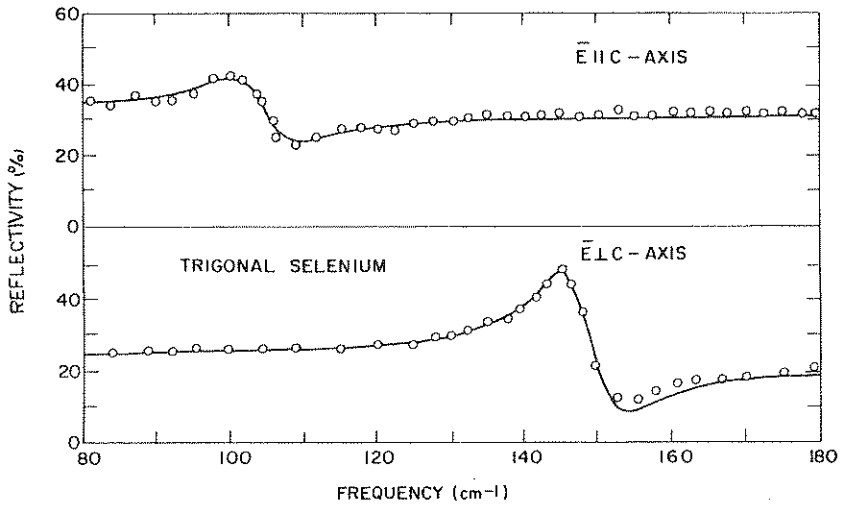

Figure 4-4 Reststrahlen spectra for trigonal Se.[21]

TABLE 4-2 ZONE-CENTER OPTICAL PHONON FREQUENCIES IN TRIGONAL Se[a]

Symmetry	Spectrum	$\bar{\nu}$ in cm^{-1}	s	γ
A_2	IR($\parallel c$)	102	0.85	0.07
E	IR($\perp c$), Raman	142	0.73	0.05
E	IR($\perp c$), Raman	231	0.02	0.04
A_1	Raman	237	—	—

[a] Refs. 15, 21, 22, and 24.

the next section. The lattice (infrared) contribution to the static dielectric constant $\varepsilon(0)$ is of the order of 1, and it is smaller than the electronic (ultraviolet) contribution, of order 10, for this crystal. For the isomorphic cousin from the next row of the periodic table, trigonal Te, the two contributions to $\varepsilon(0)$ are comparable: the lattice contribution is ≈ 10, the electronic interband contribution is ≈ 20. The reason for the stronger reststrahlen absorption in Te is the higher atomic number and consequently larger polarizability under atomic displacement.

The strong photon-phonon interaction in the reststrahlen region means that at these frequencies the true elementary excitations within the crystal are coupled electromagnetic-lattice waves. The experimental results of Figure 4-4 and Table 4-2 enable us to determine the dispersion curves for the polaritons,[6,16] the coupled photon-phonons. In Figure 4-5a is the polariton dispersion

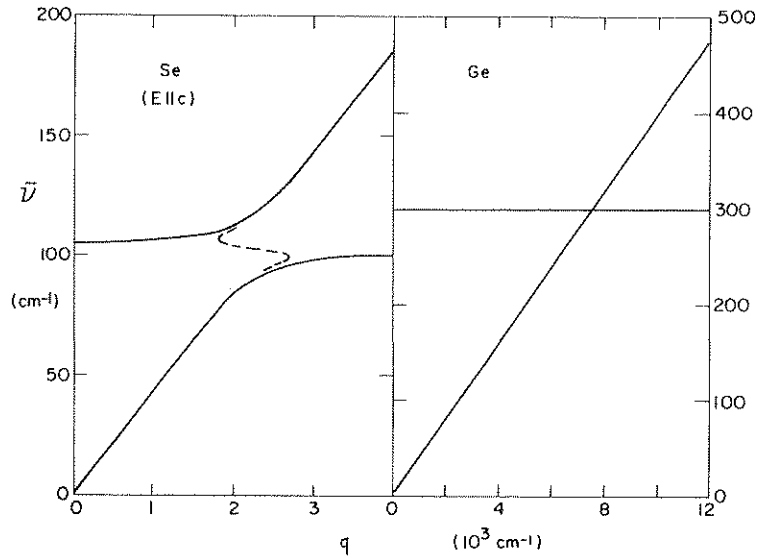

Figure 4-5 Polariton dispersion curves for Se and Ge.

curve, $\bar{\nu}(\mathbf{q})$, for the A_2 mode in Se; for comparison, the corresponding situation for Ge is shown in Figure 4-5b. In this figure, frequency is plotted against the real part of the complex propagation vector of the coupled waves. The range of $\mathbf{q}$ shown is of the order of photon wave-vectors ($\mathbf{q} \sim n\omega/c$, where n is the refractive index and ω an infrared frequency) and is small on the full scale of phonon wave-vectors ($\mathbf{q} \sim \pi/a$, where a is a lattice constant).

The dashed curve of Figure 4-5a is the experimentally-defined polariton dispersion curve; it corresponds to the oscillator parameters of Table 4-2 for $E \parallel c$, along with a high-frequency dielectric constant of 12 for this polarization.[15,21] Letting the damping constant go to zero, we obtain the solid curve shown in this figure, which displays the classical coupled-wave form.[16] The $q = 0$ intercept of the zero-damping curve locates the longitudinal-optical (LO) frequency; the $\mathbf{q} \to \infty$ asymptote determines the transverse-optical (TO) frequency.

Figure 4-5 conveys the essential difference between Se and Ge in respect to the interaction of their crystal lattices with light. For Ge, the dispersion curve consists of two intersecting straight lines: the horizontal line at the optical-phonon frequency corresponding to the pure lattice waves, and the line (of slope $1/2\pi n$) through the origin corresponding to the undisturbed light waves. The lattice waves and light waves are uncoupled, each is indifferent to the presence of the other. For Se, the two waves are coupled and the intersection between the lines is removed. The dispersion curve for Se is qualitatively similar to that of, say, NaCl. The decrease in slope between high and low frequencies of the mostly electromagnetic portions reflects the increase in dielectric constant and refractive index on passing through the reststrahlen band.

In Table 4-3, the longitudinal and transverse frequencies of the infrared-active optical phonons are compared. Also listed are the macroscopic effective charges[5] of these modes, defined by $e^* = \pi^{1/2} c m_a^{1/2} n_a^{-1/2} s^{1/2} \bar{\nu}$ where m_a is the atomic mass, n_a the number of atoms per unit volume, and s and $\bar{\nu}$

TABLE 4-3 TO AND LO FREQUENCIES, AND EFFECTIVE CHARGES OF THE INFRARED-ACTIVE PHONONS[a]

Mode	Transverse Frequency $\bar{\nu}_t$ in cm^{-1}	Longitudinal Frequency $\bar{\nu}_\ell$ in cm^{-1}	Effective Charge e^*/e	Electron-Phonon Coupling Constant
A_2	102	106	0.6	0.2
E	142	149	0.8	0.3
E	231	231	0.2	0.01

[a] Refs. 15, 21, and 22.

are the oscillator parameters of Table 4-2. These values of e^* are only about a factor of 2 smaller than the corresponding quantities for the alkali halides, demonstrating clearly that dynamic charge is no small effect.

We close our discussion of the photon-phonon interaction in trigonal Se by briefly mentioning another important "ionic" phenomenon that occurs in this crystal as a direct consequence of infrared activity: the polar-mode scattering of mobile charge carriers. Charged particles traversing the solid interact with the LO phonons via the macroscopic electric field associated with these lattice waves. The strength of the interaction is characterized by a dimensionless quantity, the electron-phonon coupling constant,[40] which is derivable from the infrared data. The coupling constants for the three LO phonons in Se are listed in the last column of Table 4-3; they are smaller than values typical of the alkali halides (≈ 5) and slightly larger than values typical of Group III–V semiconductors (≈ 0.1). Polar-mode scattering has significant influence on the electrical transport properties of trigonal Se, contributing extensively to the limitation on carrier mobilities.[21]

HIGHER ORDER OPTICAL INTERACTIONS IN TRIGONAL Se

Higher Order Phonon-Involving Optical Processes

The one-phonon optical absorption process discussed in the preceding section is the strongest and the most direct interaction between light and the crystal lattice. It is a first order process involving a single photon and a single phonon. There are a variety of weaker higher order processes coupling the lattice with electromagnetic radiation which involve the cooperation of additional elementary excitations. In this section we shall review the available experimental data on the higher order optical properties of trigonal Se which involve at least one phonon. The mechanisms for the interactions will be touched upon only briefly since, unlike the situation with respect to reststrahlen, trigonal Se does not occupy a unique role involving these interactions.

In Figure 4-6, we present a set of simple diagrams intended to introduce and illustrate the processes discussed. The direct one-phonon absorption of a far-infrared photon is represented in Figure 4-6a; Figure 4-6b–Figure 4-6e show the relevant multi-particle processes. Figure 4-6b indicates a two-phonon combination band at higher frequencies in the infrared; the annihilation of a photon is accompanied by the creation of two optical phonons. Electronic excitations and high-energy photons (i.e., visible or near-infrared) participate in the remaining three processes portrayed. A Raman scattering event is depicted in Figure 4-6c, with an incident photon virtually absorbed

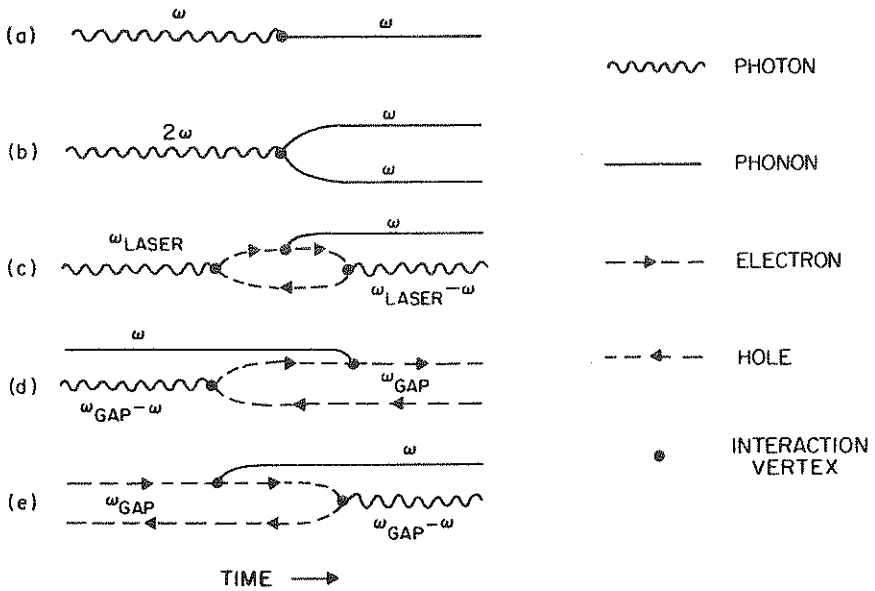

Figure 4-6 Diagrammatic representations of elementary phonon-involving optical processes: (a) one-phonon absorption (reststrahlen); (b) two-phonon absorption; (c) Raman scattering, showing a Stokes event (phonon emission); (d) phonon-assisted electronic absorption; and (e) luminescence event with emission of both photon and phonon.

and re-emitted at lower energy due to phonon emission. Figure 4-6d depicts the phonon-assisted optical creation of an electron-hole pair, while Figure 4-6e indicates the inverse process observed in luminescence.

Raman-scattering spectra for trigonal Se are reviewed in the next section, two-phonon absorption and phonon-assisted electronic optical processes are dealt with later.

Raman Scattering

Employing a YAG : Nd^{3+} laser operating at a wavelength of 1 μ, which falls within the transparent region of trigonal Se, Mooradian and Wright[24] obtained very clean scattering spectra for this crystal. A survey spectrum (unpolarized light, polycrystalline sample) exhibiting both Stokes (phonon emission) and anti-Stokes (phonon absorption) lines is shown in Figure 4-7. Clearly indicated are the three Raman-active fundamentals: the A_1 mode and the two E modes. The small TO-LO splittings of the E modes were not resolved.

The selection rules given in the last column of Table 4-1 were used to confirm the symmetry assignments. Using a single crystal and polarized incident

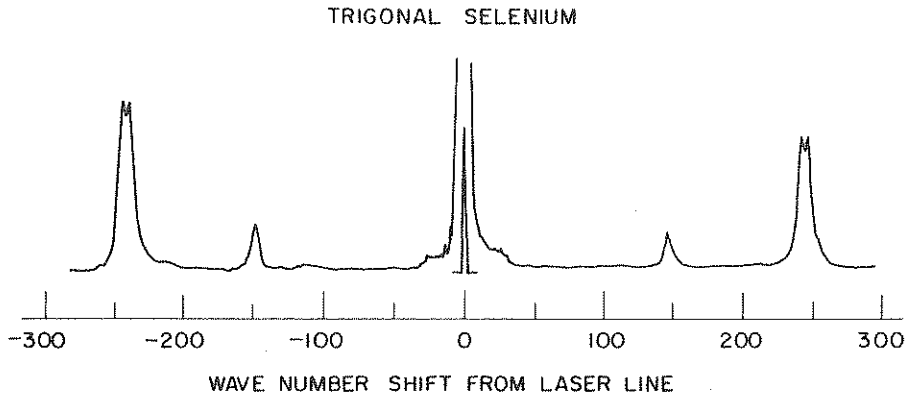

Figure 4-7 Raman scattering from trigonal Se.[24]

and scattered radiation, the A_1 line was cleanly separated from the two E lines.

Mooradian and Wright were also able to observe many weak emission bands and, in addition, determined the spectra at liquid helium temperature. One of the weak bands was identified as the Raman-forbidden A_2 fundamental, apparently weakly turned on by crystalline imperfection. The others were ascribed to scattering processes involving a pair of phonons; their frequencies are listed in Table 4-4 along with the two-phonon absorption bands to be discussed.

TABLE 4-4 SECOND ORDER SPECTRA OF TRIGONAL Se[a]

$\bar{\nu}$ in cm^{-1}	Experimental Observation		Assignment
75	—	Raman	—
102	—	Raman	A_2
130	Infrared (∥)	—	$A_1 - A_2$
183	—	Raman	—
206	—	Raman	$2A_2$
250	Infrared (⊥)	—	$A_2 + E$
275	Infrared (∥, ⊥)	Raman	$2E$
302	Infrared (⊥)	—	$3A_2$ (?)
328	Infrared (∥)	—	$A_1 + A_2$
345	—	Raman	—
365	Infrared (∥, ⊥)	—	$E + E$
438	—	Raman	$2E$
451	Infrared (⊥)	—	$A_1 + E$
455	—	Raman	$2A_1$
475	Infrared (∥, ⊥)	—	$2E$

[a] Refs. 22 and 24.

No theoretical treatment of Raman-scattering intensities in trigonal Se has yet been attempted. It is worth noting that the simple harmonic approximation shell model, employed by Chen and Zallen[10,38] for their treatment of reststrahlen in Se, is inadequate for a discussion of Raman scattering since it contains no cross term of electric field and atomic displacement. Such a bilinear term, which is equivalent to a modulation of the optical polarizability by the vibrations of the lattice, is essential to the character of the scattering mechanism. A more complicated model than the shell model would be required for a calculation of Raman intensities.

Two-Phonon Absorption

The two-phonon absorption process schematically indicated in Figure 4-6b occurs via the presence of a second order electric moment, an electric moment quadratic in the atomic displacements ($p \sim u^2$). Two different phonons may take part in this process, which can also involve phonons away from $q = 0$. Ge and Si, which have no first order moment, nevertheless exhibit weak two-phonon infrared absorption because of the existence of a second order moment.[18] Se and Te, in addition to the strong one-phonon bands produced by their first-order moments, also exhibit much weaker two-phonon bands associated with their small second order moments.

Infrared transmission measurements at photon energies above the fundamental reststrahlen region have been interpreted by Lucovsky *et al.*[22] in terms of two-phonon combination bands. Their observed frequencies, along with the analogous results from the weak second-order Raman spectra, are listed in Table 4-4. The suggested assignments are consistent with the direct-product selection rules for zone-center phonons given in Table 4-1.

Phonon-Assisted Electronic Optical Processes

The absorption edge at the electronic interband threshold in trigonal Se has been investigated by Roberts *et al.*[27] and interpreted in terms of two characteristic phonon energies. For one polarization of incident light, they observed an Urbach-rule edge with an effective phonon energy of 155 cm^{-1}; for the other polarization, they observed an indirect edge involving the cooperation of a phonon of frequency 230 cm^{-1}.

Queisser and Stuke[26] have observed a set of sharp emission lines in the luminescence spectrum of Se at low temperatures. A basic triplet of lines is replicated at lower energies, with the phonon replicas yielding a frequency of 235 cm^{-1} for the emitted phonons.

Because of the electron-phonon interaction involved in these two primarily electronic processes (Figures 4-6d and 4-6e), we would anticipate the participation of LO phonons. The lattice frequencies reported are quite close to the two *E*-mode LO-phonon frequencies given in Table 4-2.

THE SPECTRA OF MONOCLINIC Se

Structure*

Se in the α-monoclinic form is a molecular crystal made up of eight-membered ring molecules. The space group of the crystal is $P2_1/n$ (C_{2h}^5) and there are 4 molecules, 32 atoms, in the unit cell.[36] The point group of the molecule is D_{4d}. The bonding forces within the Se_8 molecule are covalent, whereas the forces holding the molecules in the monoclinic lattice are of the weaker van der Waals type. In this sense, α-monoclinic Se (which we will refer to as α-Se, for convenience) is very similar to orthorhombic sulfur. Orthorhombic S is a molecular crystal composed of S_8 molecules which have the same point-group symmetry as the Se_8 molecule.

Large single crystals of orthorhombic S are relatively easy to grow and are stable under normal ambient conditions. On the other hand, the growth of large single crystals of α-Se is at best difficult, and this structural modification of Se is metastable. Any external force, e.g., temperature, pressure, or organic vapors, tends to promote a conversion to the thermodynamically-stable trigonal modification. As a result of this stability and growth problem, α-Se has not been studied as extensively as has been orthorhombic S. For orthorhombic S, it has been well-established that the observed infrared-active[9,29] and Raman-active[32] fundamental vibrational modes are essentially those of the S_8 molecule. The unit cell of orthorhombic S contains sixteen S_8 molecules; however, there are only two types of molecules, those lying parallel to the (110) plane and those lying perpendicular to that plane.[35] The occurrence of two molecular types manifests itself in a weak crystal-field splitting of the molecular vibrational modes. The splitting is approximately 10 cm^{-1} for two of the infrared-active modes[9] and 4–5 cm^{-1} for the Raman-active modes.[32] The characteristic molecular vibrational frequencies[29] vary from about 100 cm^{-1} to 500 cm^{-1}. The ratio of the crystal field splitting to the average molecular vibrational frequency provides a measure of the ratio of the inter- and intra-molecular bonding forces. By analogy with orthorhombic S, we expect a similar relationship between the spectra of the α-Se crystal and the Se_8 molecule.

* See also Chapter 3.

Infrared Absorption

Figure 4-8 shows the transmission spectrum of a 0.2 mm thick platelet of α-Se in the region of the fundamental absorption bands, 75 cm^{-1} to 300 cm^{-1}, as measured by Lucovsky.[19] The transmission was measured with a nitrogen-purged grating spectrometer using unpolarized light and operating in a single beam mode. Three strong absorption bands were observed. Each band displays an indication of doublet splitting, with the splitting most clearly resolved in the lowest frequency band. The absorption spectrum shown here for α-Se is similar to that reported by Chantry *et al.*[9] for orthorhombic S. The sulfur work was done on pellets pressed from powdered orthorhombic S. Chantry *et al.* also studied the absorption spectrum of α-Se; however, the absorption bands they report coincide with those reported for trigonal Se,[22] indicating that their α-Se crystals underwent a thermal conversion to trigonal Se during the course of their measurements.

The absorption spectrum of the S_8 molecule has been studied in CS_2 solution.[29] The fundamental bands are essentially the same as those reported for the crystalline material with, of course, the absence of the crystal field splitting. Lucovsky studied the absorption spectrum of the Se_8 molecule in CS_2 but only observed one strong absorption band at 254 cm^{-1}, rather than

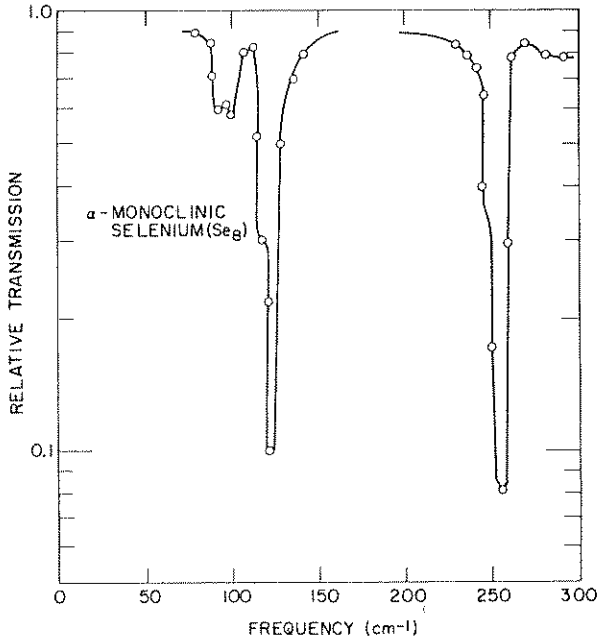

Figure 4-8 Infrared absorption of α-monoclinic Se.[19]

three as had been reported for the α-Se crystal. He also studied the second order spectrum of α-Se using unpolarized light; those results will not be discussed here.

Raman Scattering

The Raman scattering of α-Se has been reported at 300°K by Lucovsky *et al.*[22] and at 300°K and 4°K by Mooradian and Wright.[24] The low temperature spectrum of Mooradian and Wright is shown in Figure 4-9, along with their results for trigonal and amorphous Se. The spectrum of α-Se sharpens considerably as the temperature is decreased from 300°K to 4°K. Table 4-5 summarizes the vibrational frequencies of the fundamentals as obtained from the experiments performed at 300°K.[22] The symmetry assignments are

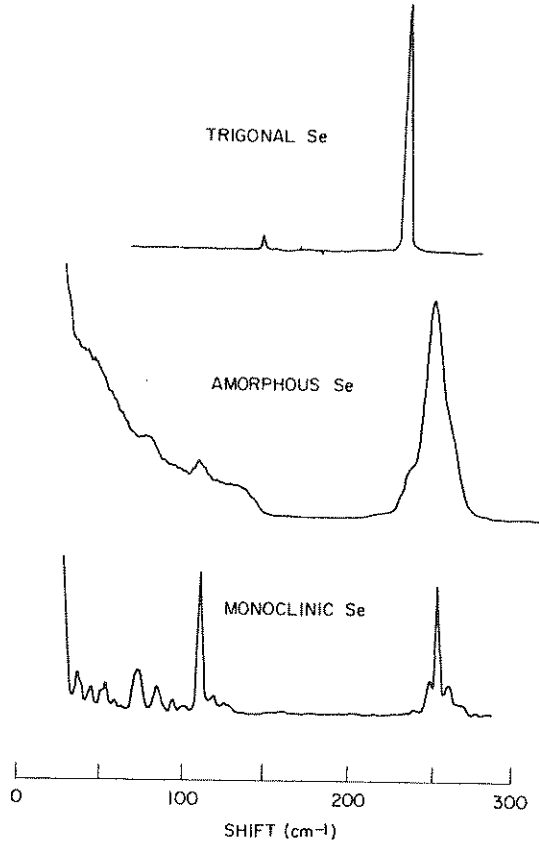

Figure 4-9 Comparison of the Raman spectra of trigonal, α-monoclinic, and amorphous Se.[24]

TABLE 4-5 SYMMETRY ASSIGNMENTS FOR THE OBSERVED FIRST ORDER INFRARED AND RAMAN SPECTRA OF Se_8 IN α-MONOCLINIC Se BASED ON THE ASSIGNMENTS FOR S_8 IN ORTHORHOMBIC S[a]

$\bar{\nu}$ in cm^{-1}	Spectrum	Assignment
50	Raman	E_2
84	Raman	E_2
92	Infrared	E_1
97	Infrared	E_1
114	Raman	A_1
116	Infrared	B_2
122	Infrared	B_2
128	Raman	E_3
239	Raman	E_3
249	Raman	A_1
254	Infrared	E_1
254	Raman	E_2

[a] Refs. 22 and 24.

based on a comparison with S_8 and are discussed in the next section. Note here that the Raman-active fundamentals of α-Se are not resolved into doublets as are the corresponding modes of S_8 in the orthorhombic S crystal.

Vibrational Assignments

Comparisons of the infrared and Raman spectra of α-Se with the corresponding spectra of orthorhombic S and the S_8 molecule suggest that the α-Se results can be discussed in terms of vibrational modes of the Se_8 molecule.

The Se_8 molecule (and also the S_8 molecule) is a puckered eight-membered ring having D_{4d} symmetry. There are eleven fundamental vibrational frequencies: $2A_1 + 3E_2 + 2E_3$ (Raman active), $B_2 + 2E_1$ (infrared active), and B_1 (inactive). The assignments[22] in Table 4-5 are based on a comparison of the α-Se lines with those of the S_8 molecule. The ratio of the vibrational frequencies of S_8 and Se_8, $\bar{\nu}(S_8)/\bar{\nu}(Se_8)$, varies between 1.72 and 2.01 with an average value of 1.9. On the basis of the ratio of the Se and S masses, a scaling factor of 1.58 is expected. The reported average value of 1.9 indicates a change in the effective molecular force constants that is consistent with the greater polarizability of the Se atom. The frequency of the inactive B_1 mode of Se_8 is estimated using the average empirical scale factor of 1.9, and it is also consistent with an assignment of the bands observed in the second order infrared absorption spectrum.

For two of the modes, the infrared measurements indicate a doublet splitting of the same relative order as that reported for the corresponding vibrational

modes of orthorhombic S. That is, according to the scaling factor of 1.9, the mode splittings in orthorhombic S are 10 cm^{-1} and 12 cm^{-1}, respectively, whereas the corresponding splittings in α-monoclinic Se are 5 cm^{-1} and 6 cm^{-1}. A splitting of the Raman-active modes was not reported for α-Se; by comparison with the splittings reported for orthorhombic S, a splitting of at most 2 to 3 cm^{-1} would be anticipated.

THE SPECTRA AND STRUCTURE OF AMORPHOUS Se*

Introduction

Prior to the recent infrared[22] and Raman[24] spectroscopy studies on amorphous selenium, a structural model for this material, based for the most part on indirect evidence, had been developed. The vitreous solid was viewed as a mixture of ring molecules and chain polymers. By analogy with the bonding forces of the crystalline modifications, the bonding of atoms within the rings and chains was considered to be covalent, and that between these units was considered to be of the weaker van der Waals type. The presence of long (more than 10^3 atoms) polymer chains was inferred from the high viscosity of Se at its melting point,[14] while the presence of rings was inferred from the partial solubility of amorphous Se in CS_2.[4] When applied to liquid Se, the polymerization theory of Eisenberg and Tobolsky[13] gave an estimate of the atomic population in Se_8 rings at the melting point of approximately 50% (see Chapter 3).

The infrared absorption spectrum of amorphous Se has been studied quite extensively.[8,31] However, prior to the recent optical experiments of Lucovsky *et al.*, the fundamental ring and chain vibrational frequencies were not known, so that an interpretation of the spectrum in terms of structural units was not possible. Nevertheless, Srb and Vasko[31] commented on similarities between the absorption spectra of orthorhombic S and amorphous Se, implying that the major features of each were due to the ring molecules.

Infrared Absorption

Figure 4-10 shows the absorption spectrum of amorphous Se in the spectral range from 50 cm^{-1} to 650 cm^{-1}.[22] Not included in the figure is a very weak absorption band at 744 cm^{-1}. The spectrum in Figure 4-10 is for a cast sample 0.2 mm thick. The spectra of evaporated samples, quenched at several substrate temperatures, were dominated by the same absorption bands with the relative absorption strengths being essentially independent of

* See also Chapter 3.

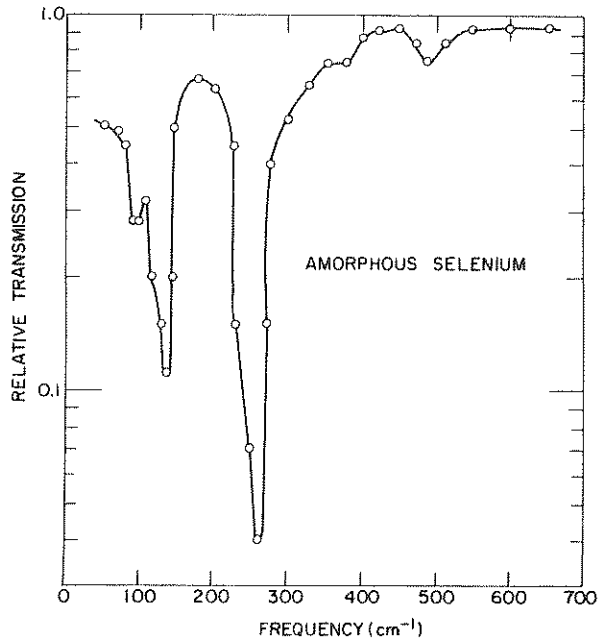

Figure 4-10 Infrared absorption of amorphous Se.[19]

the details of preparation. The dominant bands occur at 95 cm^{-1}, 135 cm^{-1}, and 254 cm^{-1}. Weaker structure is evident as two shoulders, at 120 cm^{-1} and 230 cm^{-1}, as a broad band from 280 cm^{-1} to 380 cm^{-1}, and as two weak bands at 490 cm^{-1} and 744 cm^{-1}.

Studies of the temperature dependence[22,30] of the absorption indicate that the bands at 95 cm^{-1}, 135 cm^{-1}, and 254 cm^{-1} are fundamentals, while the bands at 490 cm^{-1} and 744 cm^{-1} are second and third order combination bands, respectively.

Raman Scattering

The Raman spectrum[24] of amorphous Se has been measured at 300°K and 4°K; no sharpening of the spectrum was observed at the lower temperature. The results for 4°K are included in Figure 4-9. The Raman scattering is dominated by a very strong line at 250 cm^{-1} and a strong line at 112 cm^{-1}. Weaker structure occurs as two bands at 50 cm^{-1} and 80 cm^{-1}, and two shoulders at 135 cm^{-1} and 235 cm^{-1}. The background scattering increases with decreasing wavenumber from about 120 cm^{-1}, and is characteristic of scattering from noncrystalline solids.

The Molecular Structure of Amorphous Se

We shall first discuss the infrared absorption by developing comparisons between the spectrum of amorphous Se and those of trigonal and α-monoclinic Se. We shall then do the same for the Raman scattering. Finally, we shall summarize the infrared and Raman assignments showing that the dominant features in the reported spectra are due to vibrational modes of the Se_8 molecule.

The absorption spectrum of amorphous Se in the infrared bears a closer resemblance to that of α-Se than it does to that of trigonal Se. Figure 4-11 shows a superposition of the absorption of amorphous Se and α-Se in the region of the fundamental modes. The amorphous Se bands at 95 cm^{-1} and 254 cm^{-1} line up with the E_1 fundamentals of the Se_8 molecule as they are

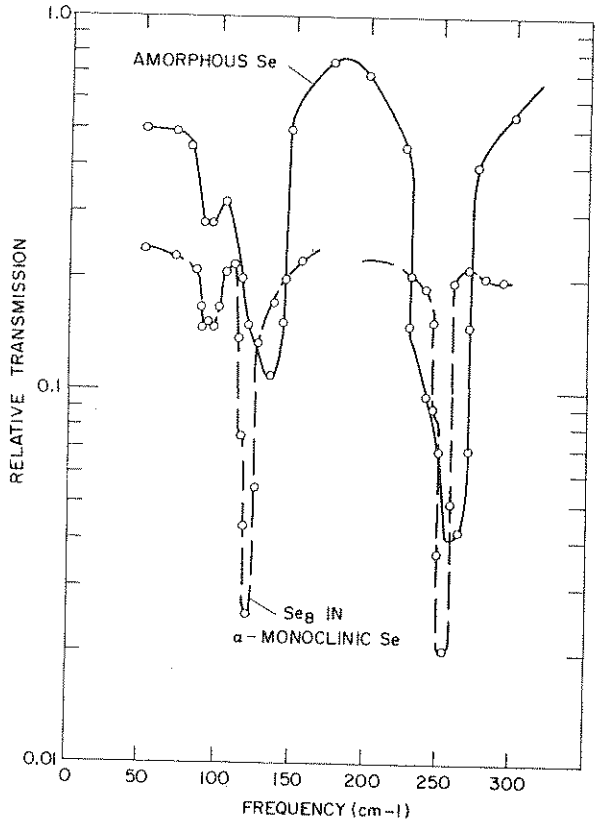

Figure 4-11 Comparison of the infrared spectrum of amorphous Se with that of Se_8 in α-monoclinic Se.[19]

reported for α-Se. The shoulder at 120 cm^{-1} in the amorphous material lines up with the third fundamental of Se_8, the B_2 mode. The bands in amorphous Se are considerably broader than those of the crystalline material, and further, they show no doublet splitting. The only strong band in amorphous Se that cannot be correlated with a fundamental in α-Se is the one at 135 cm^{-1}. This frequency is close to the trigonal Se E mode at 144 cm^{-1}; the occurrence of Raman scattering at about 138 cm^{-1} in amorphous Se prompts us to assign these spectral features near 135–140 cm^{-1} to the chain component of the amorphous solid.

The weaker features in absorption, the broad band from 280 cm^{-1} to 380 cm^{-1} and the bands at 490 cm^{-1} and 744 cm^{-1}, are also coincident with absorption bands reported for Se_8 in α-Se. In addition, the absorption in the vicinity of 490 cm^{-1} in α-Se is second order, as is the amorphous Se band. A shoulder at 230 cm^{-1} on the 254 cm^{-1} fundamental may be related to chain absorption. However, the second order spectrum of α-Se also shows structure near this energy, so that this last assignment is at best speculative.

Figure 4-9 displays an instructive comparison of the low temperature Raman spectra of amorphous Se, trigonal Se, and α-Se.[24] The dominant spectral features of the amorphous Se spectrum, at 250 cm^{-1} and 112 cm^{-1}, line up with the A_1 modes of Se_8 as they occur in α-Se. The weaker, but still resolvable, peaks at 50 cm^{-1} and 80 cm^{-1} in the amorphous Se spectrum can be attributed to E_1 vibrations of the Se_8 molecule, again by comparison with the scattering from α-Se. Based on a comparison with the scattering from trigonal Se, the shoulders in the amorphous Se spectrum at 138 cm^{-1} and 235 cm^{-1} are attributed to scattering from the polymeric chain species.

Table 4-6 summarizes the assignment of the fundamental modes of amorphous Se in terms of vibrations of the rings and chains of the crystalline modifications. Both the infrared and Raman spectra of amorphous Se are dominated by modes of the Se_8 molecule. Although Srb and Vasko[31] implied this in their comparison of the absorption of orthorhombic S and amorphous Se, the work reported here, which is based on studies of both the infrared and Raman spectra of the glass and of the two crystal forms with their different molecular units, constitutes the first definitive evidence for the presence of Se_8 molecules in amorphous Se. It would be tempting to try to estimate the relative atomic populations in the ring and chain components on the basis of the relative infrared absorption strengths and Raman scattering intensities. This is, at best, difficult because quantitative values for the absorption and scattering cross sections are not available. However, studies of the infrared absorption and Raman scattering from alloys of Se with As, S, and Te,[28] and analyses of equilibria[33,34] in the Se-S and Se-Te systems do give some insight into this question. Estimates of the atomic fraction in the Se_8 rings range from 30% to 50%; the average value of 40% being in good agreement with studies of the preferential solubility of Se_8 in CS_2. Since the average chain length is estimated to be on the order of 10^4 atoms, the ratio of rings to chains is on the order of $10^3 : 1$.

TABLE 4-6 FIRST-ORDER SPECTRA FOR AMORPHOUS Se IN TERMS OF RING AND CHAIN VIBRATIONS[a]

$\bar{\nu}$ in cm^{-1}	Spectrum	Assignment
50	Raman	Se_8, E_2
80	Raman	Se_8, E_2
95	Infrared	Se_8, E_1
112	Raman	Se_8, A_1
120	Infrared	Se_8, B_2
135	Infrared	Chain, E
138	Raman	Chain, E
235	Raman	Chain, A_1, E
250	Raman	Se_8, A_1, E_2
254	Infrared	Se_8, E_1

[a] Ref. 22.

The analysis of the infrared and Raman spectra of α-monoclinic Se indicates, as in the case of S_8 and the orthorhombic S crystal, that the bonding forces within the Se_8 molecule are considerably stronger than the intermolecular forces of the lattice. Therefore, it is expected that the vibrational frequencies of the Se_8 molecule would be relatively insensitive to the matrix in which the molecules are placed. This argument provides the basis for our interpretation of the features of the amorphous Se spectra that we associate with the Se_8 molecule. It has also been shown that the nonphotoconductive absorption in amorphous Se, in the region between 1.7 eV and 2.3 eV, can be attributed to an exciton of the Se_8 molecule.[20] The association of vibrational modes assigned to the polymer chain component of amorphous Se with modes of the trigonal Se crystal is somewhat more difficult. In trigonal Se, the axes of the helical chains are parallel to each other and the chains form an ordered hexagonal array. In amorphous Se, the chain axes are most probably not linear and the chain orientation, with respect to other chains and rings, is assumed to be random. Three of the optical modes of trigonal Se are associated with largely intrachain atomic motions: the two E modes and the A_1 mode. The restoring force and the infrared absorption strength of the A_2 mode are due to interactions with neighboring chains,[10] as discussed previously and illustrated in Figure 4-3. While the infrared and Raman spectra of amorphous Se show structure that can be attributed to the E and A_1 modes of trigonal Se, there is no evidence of the A_2 mode. This is consistent with the structural model presented here for amorphous Se.

Note Added in Proof: This review was written in July, 1970. Naturally our understanding of lattice–light interactions in the solid forms of selenium has deepened since that time. More recent developments can be found in the following two articles:

R. Zallen, In: *Proc. of the Enrico Fermi Summer School on Lattice Dynamics and Intermolecular Forces, Varenna, 1972*, S. Califano, ed., Academic Press, New York, 1973;

G. Lucovsky, In: *Proc. of the Fifth Intl. Conf. on Amorphous and Liquid Semiconductors, Garmisch-Partenkirchen, 1973*, J. Stuke, ed.

REFERENCES

1. Asendorf, R. H., *J. Chem. Phys.* **27**, 11 (1957).
2. Born, M., and Huang, K., *Dynamical Theory of Crystal Lattices*, Oxford University Press, Inc., London, 1954.
3. Born, M., and Huang, K., *ibid.*, p. 87, lines 12 and 13.
4. Briegleb, G., *Z. Phys. Chem.* **A144**, 321 (1929).
5. Burstein, E., *Lattice Dynamics*, ed., R. F. Wallis, Pergamon Press, Inc., London, 1965, p. 315.
6. Burstein, E., *Comments Solid State Phys.* **1**, 202 (1969).
7. Burstein, E., Brodsky, M. H., and Lucovsky, G., *Intern. J. Quantum Chem.* **1S**, 759 (1967).
8. Caldwell, R. S., and Fan, H. Y., *Phys. Rev.* **114**, 664 (1959).
9. Chantry, G. W., Anderson, A., and Gebbie, H. A., *Spectrochimica Acta* **20**, 1223 (1964).
10. Chen, I., and Zallen, R., *Phys. Rev.* **173**, 833 (1968).
11. Cochran, W., *Nature* **191**, 60 (1961).
12. Dick, B. G., and Overhauser, A. W., *Phys. Rev.* **112**, 90 (1958).
13. Eisenberg, A., and Tobolsky, A., *J. Polymer Sci.* **46**, 19 (1960).
14. Gee, G., *Trans. Faraday Soc.* **48**, 515 (1952).
15. Geick, R., Schroder, U., and Stuke, J., *Phys. Status Solidi* **24**, 99 (1967).
16. Huang, K., *Proc. Roy. Soc.* (*London*) **A208**, 352 (1951).
17. Hulin, M., *Ann. Phys.* (*Paris*) **8**, 647 (1963).
18. Lax, M. and Burstein, E., *Phys. Rev.* **97**, 39 (1955); Lax, M., *Phys. Rev. Letters* **1**, 131 (1958).
19. Lucovsky, G., in *Physics of Selenium and Tellurium*, ed., W. C. Cooper, Pergamon Press, Inc., Oxford, 1969, p. 255.
20. Lucovsky, G., *Proc. of Tenth Intl. Semiconductor Conf.*, 1970, USAEC, Oak Ridge, p. 799.
21. Lucovsky, G., Keezer, R. C., and Burstein, E., *Solid State Commun.* **5**, 439 (1967).
22. Lucovsky, G., Mooradian, A., Taylor, W., Wright, G. B., and Keezer, R. C., *Solid State Commun.* **5**, 113 (1967).
23. Martin, D. H., *Advan. Phys.* **14**, 39 (1965), NB p. 50.
24. Mooradian, A., and Wright, G. B., in *Physics of Selenium and Tellurium*, ed., W. C. Cooper, Pergamon Press, Inc., Oxford, 1969, p. 269.
25. Nussbaum, A., in *Solid State Physics*, Vol. 18, ed., F. Seitz and D. Turnbull, Academic Press, Inc., New York, 1966, p. 225.

26. Queisser, H. J., and Stuke, J., *Solid State Commun.* **5**, 75 (1967); Queisser, H. J., in *Physics of Selenium and Tellurium*, ed., W. C. Cooper, Pergamon Press, Inc., Oxford, 1969, p. 289.
27. Roberts, G. G., Tutihasi, S., and Keezer, R. C., *Phys. Rev.* **166**, 637 (1967).
28. Schottmiller, J., Tabak, M. D., Lucovsky, G., and Ward, A. T., *J. Non-Crystalline Solids* **4**, 161 (1970).
29. Scott, D. W., McCullough, J. P., and Druse, F. H., *J. Mol. Spectrosc.* **13**, 313 (1964).
30. Siemsen, K. J., *J. Phys. Chem. Solids* **30**, 1897 (1969).
31. Srb, I., and Vasco, A., *Czech. J. Phys.* **B13**, 827 (1963).
32. Ward, A. T., *J. Phys. Chem.* **72**, 744 (1968).
33. Ward, A. T., *J. Phys. Chem.*, **74**, 4110 (1970).
34. Ward, A. T., and Myers, M. B., *J. Phys. Chem.* **73**, 1374 (1969).
35. Warren, B. E., and Burwell, J. T., *J. Chem. Phys.* **3**, 6 (1935).
36. Wyckoff, R. W. G., *Crystal Structures* Vol. 1, Interscience Publishers, New York, 1963.
37. Zallen, R., *Phys. Rev.* **173**, 824 (1968).
38. Zallen, R., and Chen, I., in *Proc. of the Ninth Intl. Conference on the Physics of Semiconductors, Moscow*, "Nauka," Leningrad, 1968, p. 1036.
39. Zallen, R., Lucovsky, G., Taylor, W., Pinczuk, A., and Burstein, E., *Phys. Rev.* **B1**, 4058 (1970).
40. Ziman, J. M., *Electrons and Phonons*, Oxford University Press, Inc., Oxford, 1960, p. 210.

Selenium

edited by **Ralph A. Zingaro**
Department of Chemistry
Texas A & M University
College Station, Texas

and

W. Charles Cooper
United Nations Development Programme
Santiago, Chile

VNR **Van Nostrand Reinhold Company**
New York/Cincinnati/Toronto/London/Melbourne

Van Nostrand Reinhold Company Regional Offices:
New York Cincinnati Chicago Millbrae Dallas

Van Nostrand Reinhold Company International Offices:
London Toronto Melbourne

Library of Congress Catalog Card Number: 74-1246
ISBN: 0-442-29575-8

Manufactured in the United States of America
Published by Van Nostrand Reinhold Company
450 West 33rd Street, New York, N.Y. 10001

Published simultaneously in Canada by Van Nostrand Reinhold Ltd.
15 14 13 12 11 10 9 8 7 6 5 4 3 2 1

Library of Congress Cataloging in Publication Data
Zingaro, Ralph A
Selenium.
Includes bibliographies.
1. Selenium. I. Cooper, W. Charles, 1921-
joint author. II. Title.
QD181.S5Z56 546'.724'1 74-1246
ISBN 0-442-29575-8

Preface

Following the discovery of selenium by Berzelius in 1817, it was some time before a number of the physical properties of the element were noted, in particular, its photoconductivity. However, the erratic and unpredictable performance of the early photoelectric devices designed around this element led investigators to conclude that selenium had indeed been most appropriately named, being as fickle as the moon. One of the obvious characteristics of this element is, in fact, its schizophrenic chemical personality, behaving as a metallic non-metal and a non-metallic metal. This behavior is what makes this element interesting, but difficult to work with in the chemical laboratory.

Actually, it is only in more recent years that the electrical and optical properties of selenium have come to be reasonably well-understood. Thus, following the introduction of the silicon rectifier in the mid-1950's, considerable improvements in the manufacture and quality of selenium rectifiers were made. Although possibly not of commercial interest, the expitaxial growth of selenium single crystals has led